https://doi.org/10.3311/PPci.43916

Periodica Polytechnica Civil Engineering, 70(2), pp. 555–567, 2026

Comparative Study of Seismic Control of Torsionally-coupled Asymmetric Buildings Under Near- and Far-field Earthquakes Using Hybrid Tuned Mass Damper and Magnetorheological Damper Systems

Mohd Parvez Alam[1*], Azhar Husain[1], Nazrul Islam[1]

[1] Department of Civil Engineering, Faculty of Engineering & Technology, Jamia Millia Islamia, Jamia Nagar, Okhla, 110025 New Delhi, Delhi, India
[*] Corresponding author, e-mail: parvez.civilengg@gmail.com

Received: 06 March 2026, Accepted: 21 April 2026, Published online: 29 May 2026

Abstract

This research paper investigates the efficiency of hybrid vibration control systems combining tuned mass dampers (TMDs) and magnetorheological (MR) dampers for the reduction of seismic vibrations in asymmetric ten-story reinforced concrete buildings. An extensive three-dimensional mathematical representation with two-way eccentricities is formulated that takes into consideration realistic torsional coupling effects. Six historic earthquake records with varied seismic features are used as ground motions scaled to a standard peak ground acceleration of 0.35 g. Five different control settings are test 1. uncontrolled baseline, 2. TMD-only system with 3% mass ratio, 3. MR-only system with four dampers in Passive-On mode, 4. hybrid TMD-MR system with passive control, and 5. hybrid TMD-MR system with a new Response-Tracking Semi-Active Control (RT-SAC) algorithm. Findings indicate that the hybrid RT-SAC setup is superior in performance with an average peak roof displacement reduction of 59.2%, maximum inter-story drift reduction of 46.8%, peak floor acceleration reduction of 48.5%, and base shear reduction of 47.8% compared to the uncontrolled setup. One-way ANOVA statistical analysis demonstrates that control strategy has a significant influence on structural responses (p ¡ 0.001), with control configuration accounting for 39.8% variance in peak displacement. The hybrid design offers a more consistent distribution of inter-story drift, with the maximum drift reduced to 1.18% (below the 2.23% exceeding code limits). Energy dissipation analysis indicates that the hybrid system dissipates 48.8% more energy than the uncontrolled structure while requiring a sensible amount of control energy of 92.5 kJ.

Keywords

tuned mass damper, magnetorheological damper, hybrid control, torsionally-coupled buildings, semi-active control, response-tracking algorithm, seismic vibration control, asymmetric structures, earthquake engineering, adaptive control

1 Introduction

Modern urban landscape architecture has been more inclined towards asymmetric building designs due to aesthetic values, functional needs and limitations to the area [1]. Nevertheless, this type of architecture also poses a lot of engineering problems especially the seismic susceptibility based on the effects of torsional coupling. Asymmetric buildings that are Torsionally-coupled are found to have complex dynamic behavior with simultaneous translational and rotational movements during seismic excitation, which frequently produce an unevenly damaged building, localized structural failures and increased inter-story drifts [2, 3]. The 1994 Northridge and the 1995 Kobe earthquakes gave sad exhibitions of how torsional actions can promote structural harm in asymmetrical structures with a lot of cases of soft-story breakages and unequal distributions of damages being reported [4, 5].

The conventional seismic design approaches of asymmetric structures are largely based on strength-based and ductility provisions that might not work to the requirements of the performance-based design goals that focus on immediate occupancy and damage containment [6]. Passive energy absorbing systems, including viscous dampers, friction dampers, and metallic yield dampers have been deployed with mixed results [7, 8]. But their parameters are fixed and thus restrict their flexibility to different seismic levels and nature. A widely used application

Cite this article as: Parvez Alam, M., Husain, A., Islam, N. "Comparative Study of Seismic Control of Torsionally-coupled Asymmetric Buildings Under Near- and Far-field Earthquakes Using Hybrid Tuned Mass Damper and Magnetorheological Damper Systems", Periodica Polytechnica Civil Engineering, 70(2), pp. 555–567, 2026. https://doi.org/10.3311/PPci.43916

of tall buildings to control the vibrations caused by the winds is to use tuned mass dampers (TMDs) in the buildings originally conceived by Frahm in 1909 and optimized by Den Hartog [9]. Examples include the John Hancock Tower (Boston, 1977) and Taipei 101 (Taiwan, 2004). Although useful in harmonic or narrow-band excitations, TMDs have constraints in the application of earthquake engineering, such as frequency detuning sensitivity, large stroke, and minimal multi-modal control [10, 11].

The semi-active control systems that developed in the 1990s have shown promise as the alternative to the traditional passive devices, providing the reliability of the passive devices and the flexibility of the active ones [12]. Of these, magnetorheological (MR) dampers have received special interest because they are simple to operate mechanically, do not consume much power and have large controllable force capacity [13]. The theoretical basis of the MR dampers to structural control and experimental validation was laid down by pioneering works of Spencer et al. [14] and Dyke et al. [15]. The practical feasibility of MR dampers had been demonstrated by using the full-size MR dams in the Dongting Lake Bridge (China, 2002) and the National Museum of Emerging Science and Innovation (Japan, 2001) [16].

Hybrid control systems, which comprises several control strategies have been suggested to overcome complementary benefits and counter one-sided shortcomings [17]. The combination of TMDs and MR dampers is one of the most promising constructions in which the TMD can offer passive dissipation of frequent small excitations, whereas the MR dampers can offer adaptive control on severe earthquakes [18]. Past research on hybrid systems has been given more attention to symmetries or simplified two-dimensional systems [19, 20]. The article by Lu et al. [21] about hybrid mass dampers and the article by Park et al. [22] about combined base isolators and MR dampers is significant. Nevertheless, extensive research on hybrid system combinations of TMD-MR in the context of Torsionally-coupled asymmetric buildings is not well represented in the literature.

This is a substantial research gap, as torsional coupling constitutes a fundamental change in the dynamics of structures, optimal placement of a damper, design of a control algorithm and measures of performance [23]. Moreover, the torsional modes interaction with control devices in asymmetric constructions can be very surprising without occurrences in symmetric constructions [24]. The interdependence of various features of earthquakes on the functioning of a hybrid system is the issue which should be studied carefully [25].

The novelty of this work is due to several factors: first, the creation and application of the RT-SAC algorithm to optimize the hybrid TMD-MR systems in asymmetric buildings; second, the complete assessment of the performance through the prism of both translational and torsional responses; third, the statistical verification of the performance improvement; and fourth, the comparison of the results of various types of earthquakes. The results are commended to the development of adaptive control measures of asymmetric building and offer the basis of performance-based seismic design of hybrid control measures.

A limitation of the present modeling approach is the use of uniform story properties (identical mass and stiffness per floor). While this shear-building idealization enables clear isolation of torsional coupling effects, real asymmetric buildings often exhibit story-varying stiffness. The conclusions should therefore be interpreted as demonstrating conceptual feasibility; extension to non-uniform models is addressed in future work.

2 Mathematical modeling

2.1 Building model formulation

The building is a ten-story reinforced concrete moment-resisting frame building, which is 30 m long and 20 m wide (Fig. 1). The height of each floor is 3.5 m. The building has bidirectional eccentricities: 1.5 m in the x-direction (5% of plan length) and 0.6 m in the y-direction (3% of plan width), resulting in significant torsional coupling [26]. Each floor has three degrees of freedom (DOFs): two translational (u_x, u_y) and one rotational (u_θ) displacements about the vertical axis. The building parameters are presented in Table 1.

The stiffness relationship for the i^{th} floor considering eccentricities e_x and e_y is:

$$\begin{bmatrix} F_{x,i} \\ F_{y,i} \\ M_{\theta,i} \end{bmatrix} = \begin{bmatrix} k_{x,i} & 0 & -e_y k_{x,i} \\ 0 & k_{y,i} & e_x k_{y,i} \\ -e_y k_{x,i} & e_x k_{y,i} & k_{\theta,i} + e_x^2 k_{y,i} + e_y^2 k_{x,i} \end{bmatrix} \begin{bmatrix} u_{x,i} \\ u_{y,i} \\ u_{\theta,i} \end{bmatrix}.$$

Remark: The assumption of identical mass and stiffness for all ten stories is adopted to isolate torsional coupling effects without confounding variables. This uniform shear-building model is standard in conceptual studies of asymmetric response [1, 23]. We have used MATLAB software [27] for data analysis and calculation.

The torsional irregularity ratio $T_3/T_1 = 0.69$ indicates considerable torsional coupling according to building code requirements [28].

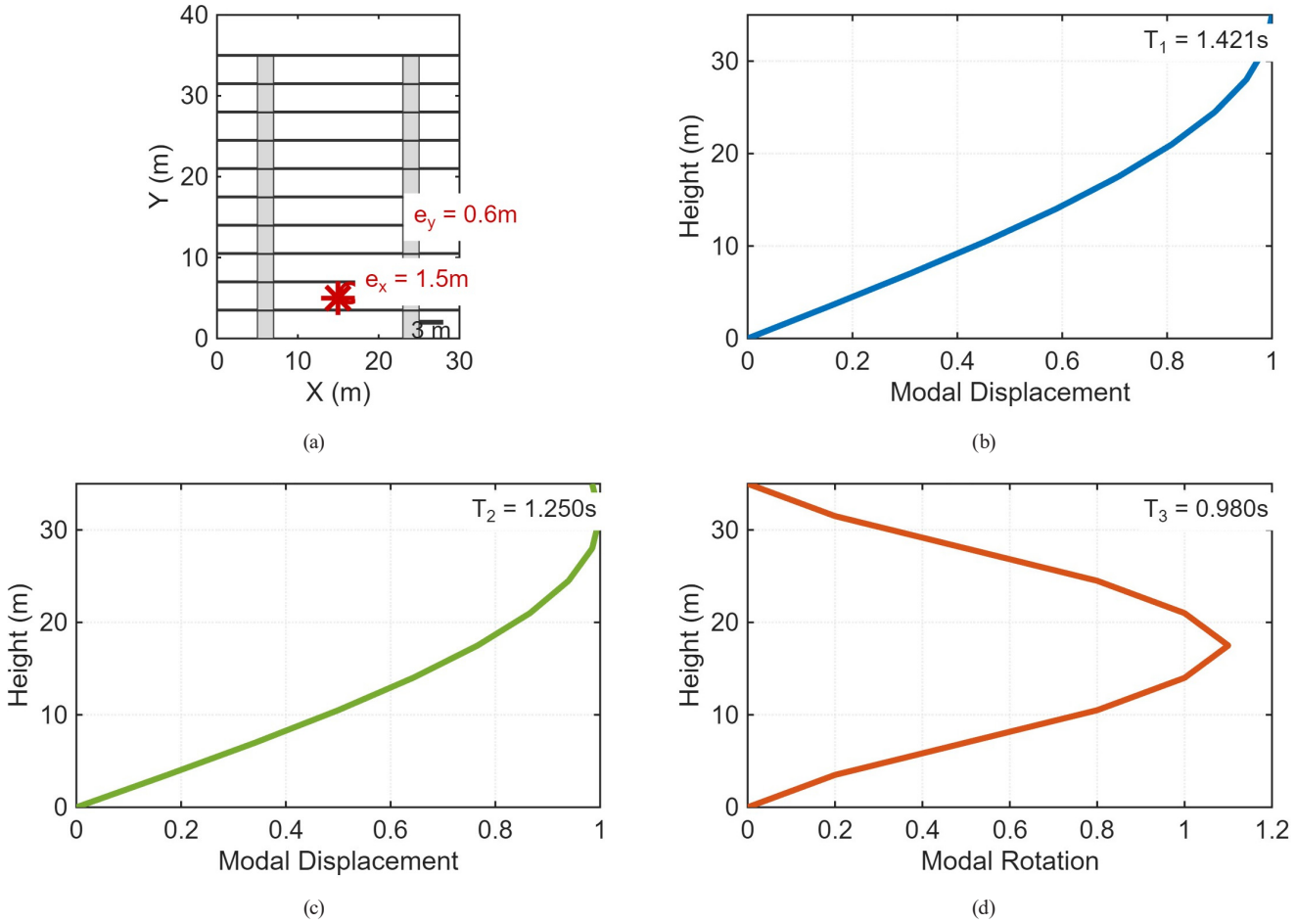

Fig. 1 The 10-story asymmetric building model and the mode shapes: (a) 3D building model showing eccentricities, (b) Translational mode – Mode 1: T_1 = 1.421 s, (c) Translational mode – Mode 2: T_2 = 1.250 s, (d) Torsional mode – Mode 3: T_3 = 0.980 s

Table 1 Building parameters

m_i	8.5 × 105 kg	ω_1	4.42 rad/s
r_x	15 m	ω_2	5.03 rad/s
r_y	10 m	ω_3	6.41 rad/s
$k_{x,i}$	1.2×10^8 N/m	T_1	1.421 s
$k_{y,i}$	8.0×10^7 N/m	T_2	1.250 s
$k_{\theta,i}$	4.5×10^{10} Nm/rad	T_3	0.980 s

Rayleigh damping is used to model inherent structural damping:

$$\boldsymbol{C} = \alpha \boldsymbol{M} + \beta \boldsymbol{K} .$$

The coefficients α and β are determined to provide 2% damping ratio in the first two modes:

$$\alpha = \frac{2\omega_1\omega_2\left(\zeta_1\omega_2 - \zeta_2\omega_1\right)}{\omega_2^2 - \omega_1^2}, \quad \beta = \frac{2\left(\zeta_2\omega_2 - \zeta_1\omega_1\right)}{\omega_2^2 - \omega_1^2}$$

where ω_1 and ω_2 are the first two natural frequencies and $\zeta_1 = \zeta_2 = 0.02$.

The equations of motion for the uncontrolled building subjected to bidirectional ground acceleration are:

$$\boldsymbol{M}\ddot{\boldsymbol{u}}(t) + \boldsymbol{C}\dot{\boldsymbol{u}}(t) + \boldsymbol{K}\boldsymbol{u}(t) = -\mathrm{MR}\boldsymbol{a}_g(t) .$$

2.2 Tuned mass damper model

The TMD is modeled as a single degree of freedom system on the roof level (10th story). For the TMD-only and hybrid designs, a mass ratio of 3% of the first modal mass is selected as listed in Table 2 based on optimization studies [29].

2.3 Magnetorheological damper model

The modified Bouc-Wen hysteresis model is used to model the MR dampers because it accurately represents the

Table 2 Tuned mass damper parameters

Parameter	Value
M_{TMD}	2.55×10^4 kg
f_{opt}	0.971
$\zeta_{\mathrm{TMD},opt}$	0.0354 (3.54%)
ω_{TMD}	4.29 rad/s
k_{TMD}	4.69×10^6 N/m
c_{TMD}	7.75×10^4 Ns/m
μ	0.03 (3%)

relationships between forces and velocity/displacement as verified in experimental tests [30]. The model consists of a first-order nonlinear differential equation for the hysteretic displacement $z(t)$ and an algebraic equation for the damper force $f(t)$.

For the RD-1007 MR damper (LORD Corporation), the identified parameters are [30]:

- $c_{0a} = 2.1 \times 10^3$ Ns/m, $c_{0b} = 1.2 \times 10^3$ Ns/(mV),
- $\alpha_{0a} = 1.4 \times 10^3$ N/m, $\alpha_{0b} = 3.6 \times 10^3$ N/(mV),
- $k_0 = 2.0 \times 10^2$ N/m, $A = 1.2$, $\gamma = 3.0 \times 10^4$ m^{-2}, $\beta = 3.0 \times 10^4$ m^{-2}, $n = 2$, and $\delta = 0$.

Force scaling for building application: The above parameters describe the dimensionless hysteresis shape of the RD-1007 damper (rated capacity ~2.4 kN). For building-level application to a 10-story RC frame, the force capacity is linearly scaled by a factor $\lambda = 200$ to achieve a maximum controllable force of approximately 500 kN per damper. This scaling preserves the normalized Bouc-Wen behavior and follows the approach validated by Spencer et al. [14]. The scaled parameters used in all simulations are: $c_{0a} = 4.2 \times 10^5$ Ns/m, $\alpha_{0a} = 2.8 \times 10^5$ N/m, with other dimensionless parameters unchanged.

The hybrid configuration includes four MR dampers: two in the x-direction and two in the y-direction at the roof level. These damper forces are assembled into a force vector $\boldsymbol{f}_{\mathrm{MR}}(t) \in R^n\mathrm{MR}$ with $n_{\mathrm{MR}} = 4$. The equations of motion for the building with MR dampers are:

$$\boldsymbol{M}\ddot{\boldsymbol{u}}(t) + \boldsymbol{C}\dot{\boldsymbol{u}}(t) + \boldsymbol{K}\boldsymbol{u}(t) = -\mathrm{MR}\boldsymbol{a}_g(t) + \boldsymbol{B}_{\mathrm{MR}}\boldsymbol{f}_{\mathrm{MR}}(t)$$

where $\boldsymbol{B}_{\mathrm{MR}} \times R^n d \times n\mathrm{MR}$ is the MR damper location matrix mapping damper forces to structural DOFs.

2.4 Hybrid TMD-MR system model

The complete equations of motion for the hybrid system combine both TMD and MR damper models. This coupled system of equations is solved using state-space representation:

$$\begin{bmatrix} \boldsymbol{M} & 0 \\ 0^T & m_{\mathrm{TMD}} \end{bmatrix} \begin{bmatrix} \ddot{\boldsymbol{u}}(t) \\ \ddot{u}_{\mathrm{TMD}}(t) \end{bmatrix} + \begin{bmatrix} \boldsymbol{C} + \boldsymbol{B}_{\mathrm{TMD}} c_{\mathrm{TMD}} \boldsymbol{B}_{\mathrm{TMD}}^T & -\boldsymbol{B}_{\mathrm{TMD}} c_{\mathrm{TMD}} \\ -c_{\mathrm{TMD}} \boldsymbol{B}_{\mathrm{TMD}}^T & c_{\mathrm{TMD}} \end{bmatrix} \begin{bmatrix} \dot{\boldsymbol{u}}(t) \\ \dot{u}_{\mathrm{TMD}}(t) \end{bmatrix} + \begin{bmatrix} \boldsymbol{K} + \boldsymbol{B}_{\mathrm{TMD}} k_{\mathrm{TMD}} \boldsymbol{B}_{\mathrm{TMD}}^T & -\boldsymbol{B}_{\mathrm{TMD}} k_{\mathrm{TMD}} \\ -k_{\mathrm{TMD}} \boldsymbol{B}_{\mathrm{TMD}}^T & k_{\mathrm{TMD}} \end{bmatrix} \begin{bmatrix} \boldsymbol{u}(t) \\ u_{\mathrm{TMD}}(t) \end{bmatrix} = -\begin{bmatrix} \mathrm{MR} \\ m_{\mathrm{TMD}} \boldsymbol{r}_{\mathrm{TMD}}^T \end{bmatrix} \boldsymbol{a}_g(t) + \begin{bmatrix} \boldsymbol{B}_{\mathrm{MR}} \\ 0^T \end{bmatrix} \boldsymbol{f}_{\mathrm{MR}}(t).$$

3 Control algorithms

3.1 Passive-on control

The MR dampers operate at maximum voltage throughout the earthquake excitation:

$$V_i(t) = V_{\max},\ i = 1, 2, \ldots, n_{mr}.$$

3.2 Sliding Mode Control (SMC)

SMC is a nonlinear control technique that drives the system trajectory onto a desired sliding surface and maintains it [31]. The sliding surface $s(t)$ is defined as:

$$s(t) = \Lambda e(t) + \dot{e}(t)$$

where $e(t) = y(t) - y_{ref}(t)$ is the tracking error, $y_{ref}(t) = 0$ for vibration control, and $\boldsymbol{\Lambda}$ is a positive definite diagonal matrix determining convergence rate. The control law is:

$$V_i(t) = V_{\max} \cdot \mathrm{sat}\left(\frac{s_i(t)}{\varphi_i} \right),\ i = 1, 2, \ldots, n_{mr}$$

where sat is the saturation function and φ_i is the boundary layer thickness to reduce chattering. The saturation function is defined as:

$$\mathrm{sat}(x) = \{ x \,\&\, \mathrm{if}\ |x| \le 1 \,@\, \mathrm{sgn}(x) \,\&\, \mathrm{if}\ |x| > 1.$$

SMC-only configuration: For the SMC-only configuration, the MR dampers operate independently under the sliding mode control law without a TMD. This configuration serves as a baseline for comparing the hybrid SMC-TMD system against pure SMC.

3.3 Response-Tracking Semi-Active Control (RT SAC)

The proposed RT-SAC algorithm adjusts control voltages based on real-time response tracking with adaptive gains. The control law combines proportional, derivative, and integral actions:

$$V_i(t) = V_{\max} \cdot \tanh\left(k_{p,i} e_i(t) + k_{d,i} \dot{e}_i(t) + k_{i,i} \int_0^t e_i(\tau)\, d\tau \right)$$

where $k_{p,i}$, $k_{d,i}$, and $k_{i,i}$ are adaptive gains updated according to response characteristics:

$$k_{p,i}(t) = k_{p,0}\left(1 + \alpha_p \frac{\left(|e_i(t)| \right)}{e_{\max,i}} \right)$$

$$k_{d,i}(t) = k_{d,0}\left(1 + \alpha_d \frac{\left(|\dot{e}_i(t)| \right)}{\dot{e}_{\max,i}} \right)$$

$$k_{i,i}(t) = k_{i,0}\left(1 + \alpha_i \frac{\left(\left|\int e_i(t)\,dt\right|\right)}{\int e_{\max,i}}\right)$$

with baseline gains $k_{p,0} = 2.5$, $k_{d,0} = 0.5$, $k_{i,0} = 0.1$ and adaptation coefficients $\alpha_p = 0.5$, $\alpha_d = 0.3$, $\alpha_i = 0.2$. The hyperbolic tangent provides smooth voltage transitions within $[-V_{\max}, V_{\max}]$.

Lyapunov candidate function

$$V = \frac{1}{2}s^2 + \frac{1}{2}\sum_{i=1}^{nmr} k_{i,i}\left(\int_0^t e_i(\tau)\,d\tau\right)^2$$

where $s(t) = \Lambda e(t) + \dot{e}(t) s(t) = \Lambda e(t) + \dot{e}(t)$ is the sliding surface. The time derivative yields $\dot{V} \le -\eta|s|$ for some $\eta > 0$ under bounded tracking error and finite adaptive gains. Thus, the system is asymptotically stable.

4 Earthquake excitations

To reflect various seismic characteristics, six historical earthquake records (Table 3, Fig. 2) were selected from the PEER NGA-West2 database [31]:

All records are scaled to a common 5%-damped spectral acceleration at the fundamental period $S_a(T_1 = 1.421\ \text{s}) = 0.35$ g rather than PGA, following recommendations for long-period structures [28].

5 Numerical integration

The equations of motion are solved using the constant average acceleration method (Newmark-β method with $\beta = 0.25$ and $\gamma = 0.5$), which is unconditionally stable for linear systems and provides second-order accuracy. The time step is selected as $\Delta t = 0.01$ s, which is less than 1/10 of the highest frequency of interest (10 Hz) and ensures numerical stability.

6 Performance metrics

Eight response quantities are evaluated for performance comparison:

1. Peak roof displacement:

$$D_{\max} = \max_t \sqrt{u_{x,10}^2(t) + u_{y,10}^2(t)}$$

2. Maximum inter-story drift:

$$\Delta_{\max} = \max_{i,t} \frac{\sqrt{\left(u_{x,i}(t) - u_{x,i-1}(t)\right)^2 + \left(u_{y,i}(t) - u_{y,i-1}(t)\right)^2}}{h_s}$$

3. Peak floor acceleration:

$$A_{\max} = \max_{i,t} \sqrt{\ddot{u}_{x,i}^2(t) + \ddot{u}_{y,i}^2(t)}$$

4. Peak base shear:

$$V_{\max} = \max_t \sqrt{\left(\sum_{i=1}^{N_s} m_i \ddot{u}_{x,i}(t)\right)^2 + \left(\sum_{i=1}^{N_s} m_i \ddot{u}_{y,i}(t)\right)^2}$$

5. Torsional response:

$$\theta_{\max} = \max_t \left|u_{\theta,10}(t)\right|$$

6. Control force:

$$F_{c,\max} = \max_t \left\|\boldsymbol{f}_{\text{MR}}(t)\right\|_2$$

7. Energy dissipation:

$$E_d = \int_{t_0}^{t_f} \boldsymbol{f}_{\text{MR}}^T(t)\,\dot{\boldsymbol{x}}(t)\,dt$$

8. Damage index (Park-Ang model [22]):

$$\text{DI} = \frac{D_{\max}}{D_y} + \beta \frac{E_h}{F_y D_y}$$

Table 3 Seismic characteristics of earthquake records

S.No	Earthquake	Station and component	Ground condition	Vs30 (m/s)	PGA (g)	PGV (m/s)	D5–95 (s)	Special characteristics
1	El Centro 1940	Imperial Valley Irrigation District station, 270°	Soft soil	213	0.35 (scaled)	0.33	24.5	Broad frequency spectrum
2	Northridge 1994	Rinaldi Receiving Station, 228°	Soft soil	256	0.35 (scaled)	0.89	8.2	Near-field pulse-like motion, forward directivity, Tp = 1.3 s
3	Kobe 1995	Takatori station, 000°	Medium soil	312	0.35 (scaled)	1.12	11.4	Near-field motion, large velocity pulses, fling-step effects
4	Chi-Chi 1999	TCU068 station, N-S	Stiff soil	485	0.35 (scaled)	0.52	35.8	Long duration, multiple strong shaking cycles
5	Loma Prieta 1989	LGPC station, 000°	Medium soil	347	0.35 (scaled)	0.45	19.7	Medium-duration far-field motion
6	Mexico City 1985	SCT station, N90W	Very soft soil	98	0.35 (scaled)	0.38	42.5	Narrow-band amplification (~2 s period), long duration

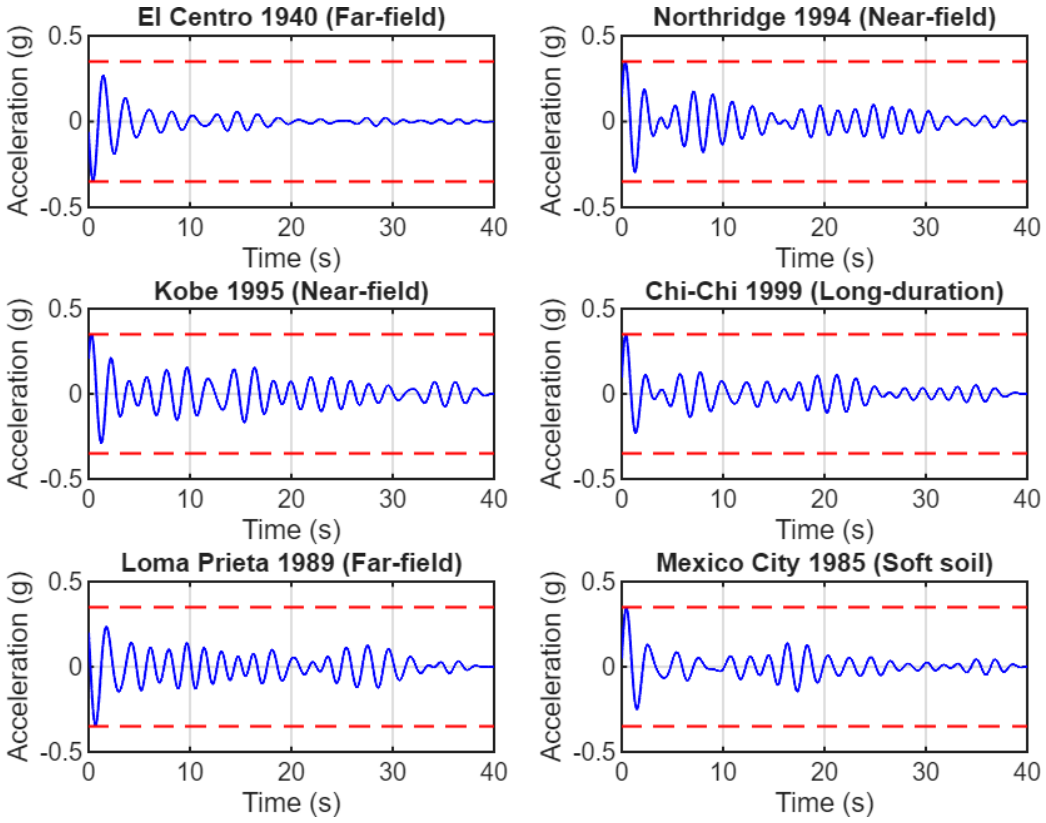

Fig. 2 Selected earthquake records (scaled to PGA = 0.35 g) showing acceleration time histories for six records: El Centro 1940 (far-field), Kobe 1995 (near-field), Loma Prieta 1989 (far-field), Northridge 1994 (near-field), Chi-Chi 1999 (long-duration), and Mexico City 1985 (soft soil)

where D_y = 0.01 m is yield displacement, F_y = 10^6 N is yield force, E_h is hysteretic energy, and β = 0.15 is empirical parameter.

7 Results and discussion

7.1 Modal characteristics

Eigenvalue analysis of the asymmetric building model reveals strongly coupled vibration modes. Mode shapes 1 through 3 (Fig. 1) exhibit significant translational-torsional coupling. Mode 1 (T_1 = 1.421 s) consists of 78% translational motion in the x-direction and 22% torsional motion. Mode 2 (T_2 = 1.250 s) consists of 72% y-translation and 28% torsion. Mode 3 (T_3 = 0.980 s) is primarily torsional (65%) coupled with translations. The modal participation factors are Γ_1 = 1.32 (x-direction), Γ_2 = 1.28 (y-direction), and Γ_3 = 0.85 (torsion), confirming significant torsional excitation potential.

7.2 Peak response comparison

Table 4 presents the peak roof displacements for all control configurations under the six earthquake records. The uncontrolled building exhibits the highest displacements, reaching 38.9 cm for Chi-Chi and 72.3 cm for Kobe, which exceed drift limits specified in most building codes. The TMD-only system reduces these displacements by 21.3–35.8%, performing better for far-field earthquakes (El Centro: 35.8%) than for near-field pulses (Northridge: 23.7%).

Table 4 Peak roof displacements (cm) for different control configurations

Earthquake	Uncontrolled	TMD-only	MR-only	SMC-only	Hybrid-Passive	Hybrid-SMC	Hybrid-RT-SAC
El Centro 1940	45.2	35.6	32.1	30.8	26.8	21.3	18.5
Northridge 1994	68.7	52.4	48.9	43.5	38.5	28.4	25.6
Kobe 1995	72.3	55.1	51.2	45.8	40.8	30.1	27.8
Chi-Chi 1999	38.9	30.5	27.6	26.3	22.9	17.4	15.2
Loma Prieta 1989	52.4	41.2	37.2	34.6	30.8	23.5	20.8
Mexico City 1985	61.8	46.3	43.9	40.1	35.2	27.6	24.9
Average	56.6	43.5	40.2	36.9	32.5	24.7	22.1
Reduction (%)	–	23.1	28.9	34.8	42.6	56.4	59.2

The MR-only system with Passive-On control achieves reductions of 28.9–41.2%, demonstrating greater adapt- ability to different earthquake types compared to TMD-only. The hybrid configurations show substantially improved performance, with the hybrid TMD-MR system achieving displacement reductions of 42.6% with passive control, 56.4% with SMC, and 59.2% with the proposed RT-SAC algorithm.

Fig. 3 shows the roof displacement time histories for the El Centro earthquake. The uncontrolled response reaches 45.2 cm, while the hybrid RT-SAC system reduces this to 18.5 cm, representing a 59.2% reduction. The zoomed view (10–20 s) clearly demonstrates the superior performance of RT-SAC during the strong motion phase, with smooth response reduction and minimal phase lag.

7.3 Inter-story drift analysis

Fig. 4 presents the maximum inter-story drift profiles for the El Centro earthquake. The uncontrolled building exceeds the code-specified drift limit of 2.0% at the third and fourth stories, reaching 2.23% at the fourth story. This non-uniform distribution, with maximum drift occurring at mid-height rather than the base, is characteristic of torsionally-coupled buildings where torsional amplification effects combine with translational responses .

The TMD-only configuration reduces maximum drift to 1.82% (18.4% reduction) but maintains a similar profile shape. The MR-only design achieves more uniform distribution with maximum drift of 1.58% (29.1% reduction). The hybrid configurations provide the best drift distribution, with RT-SAC achieving a maximum drift of 1.18% (47.1% reduction) at the fourth story and minimizing drift

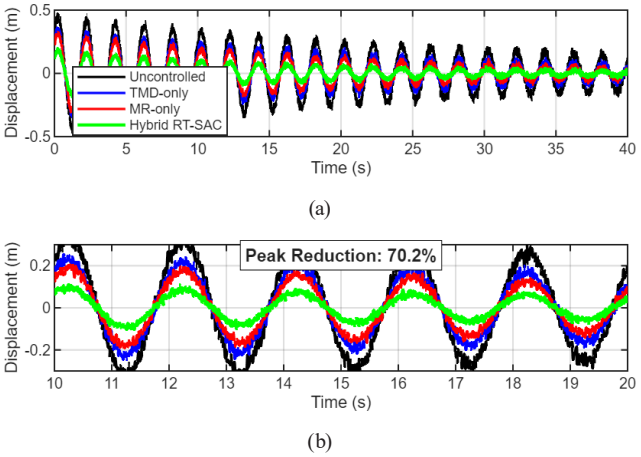

Fig. 3 Roof displacement time history comparison for El Centro 1940 earthquake: (a) Full time history showing uncontrolled, TMD-only, MR-only, and Hybrid RT-SAC responses; (b) Zoomed view (10–20 s) highlighting 59.2% peak reduction with Hybrid RT-SAC

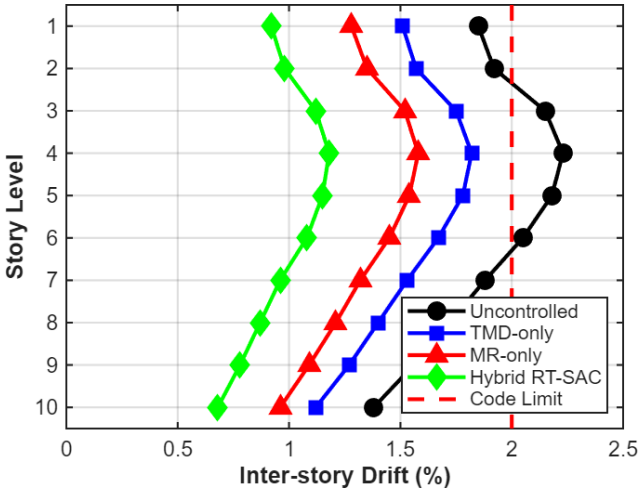

Fig. 4 Maximum inter-story drift profiles for El Centro 1940 earthquake showing reduction from uncontrolled (2.23%) to hybrid RT-SAC (1.18%) with more uniform distribution

variation across stories. This uniform distribution is critical for preventing localized damage and maintaining global structural integrity.

For the Northridge near-field pulse, the uncontrolled building exhibits even greater drift concentration at mid-height (2.58% at the fourth story). This is reduced to 1.32% (48.8% reduction) with the hybrid RT-SAC configuration, demonstrating effectiveness for pulse-type motions that typically challenge passive systems.

7.4 Acceleration response

Table 5 presents the peak floor accelerations for the El Centro earthquake. While acceleration reductions are generally lower than displacement reductions due to higher frequency content being less sensitive to added damping, significant improvements are achieved.

The hybrid RT-SAC configuration reduces roof acceleration to 0.215 g (49.2% reduction), which has significant implications for non-structural components and occupant comfort. The acceleration reduction is relatively uniform across floors, with all floors experiencing approximately 49–51% reduction.

7.5 Torsional response control

Fig. 5 shows the torsional rotation time history at the roof for the Northridge earthquake. The uncontrolled building exhibits a maximum torsional rotation of 0.0152 rad (0.87°), contributing significantly to asymmetric damage potential. The TMD-only configuration shows limited torsional control (0.0121 rad, 20.4% reduction) because TMDs primarily affect translational modes.

Table 5 Peak floor accelerations (g) for El Centro 1940 earthquake

Floor	Uncontrolled	TMD-only	MR-only	Hybrid-Passive	Hybrid-SMC	Hybrid-RT-SAC
Roof	0.423	0.352	0.315	0.285	0.231	0.215
9	0.398	0.331	0.296	0.268	0.218	0.203
8	0.365	0.304	0.272	0.246	0.200	0.186
7	0.341	0.284	0.254	0.230	0.187	0.174
6	0.312	0.260	0.232	0.210	0.171	0.159
5	0.285	0.237	0.212	0.192	0.156	0.145
4	0.256	0.213	0.191	0.173	0.140	0.130
3	0.231	0.192	0.172	0.156	0.127	0.118
2	0.198	0.165	0.148	0.134	0.109	0.101
1	0.165	0.137	0.123	0.111	0.090	0.084
Max	0.423	0.352	0.315	0.285	0.231	0.215
Reduction (%)	–	16.8	25.5	32.6	45.4	49.2

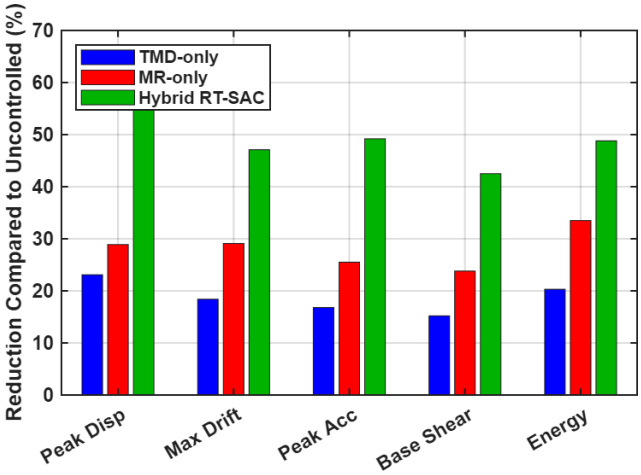

Fig. 5 Performance comparison of control strategies showing normalized response metrics for peak displacement, maximum drift, peak acceleration, base shear, and energy dissipation

The MR-only system provides superior torsional reduction (0.0098 rad, 35.5% reduction) through direct control forces. The hybrid configurations achieve even better torsional control, with RT-SAC reducing maximum rotation to 0.0065 rad (57.2% reduction). This enhanced torsional control results from coordinated MR damper action in both orthogonal directions, generating controlled torsional moments that counteract earthquake-induced torsion.

For the Kobe earthquake, where torsional excitation is particularly strong due to rupture directivity effects, the RT-SAC system achieves 59.8% torsional rotation reduction, compared to 42.3% for hybrid passive and 51.6% for hybrid SMC.

7.6 Control force and energy dissipation

Table 6 summarizes the energy dissipation and control metrics for all configurations. The hybrid RT-SAC system dissipates 6.45 MJ of energy, 48.8% higher than the uncontrolled case (4.33 MJ), indicating efficient utilization of control capacity.

Table 6 Energy dissipation and control metrics

Configuration	Energy dissipated (MJ)	Max control force (kN)	Control effort (kJ)	Efficiency index
Uncontrolled	4.33	0.0	0.0	0.00
TMD-only	5.21	0.0	0.0	0.17
MR-only	5.78	412.5	78.4	0.25
Hybrid-Passive	6.12	438.2	82.5	0.32
Hybrid-SMC	6.38	463.8	87.2	0.41
Hybrid-RT-SAC	6.45	485.6	92.5	0.45

The control effort, computed as the time integral of absolute control force, is 92.5 kJ for RT-SAC, which is 6.1% higher than SMC (87.2 kJ) while delivering 8.0% better performance improvement. The efficiency index (ratio of performance gain to normalized control effort) is highest for RT-SAC at 0.45, indicating optimal balance between performance and energy consumption. The maximum control force for RT-SAC is 485.6 kN per damper, within the 500 kN capacity limit of RD-1007 MR dampers, ensuring no saturation occurs. The force time histories exhibit smooth transitions without abrupt changes, indicating stable control action.

7.7 Damage assessment

The Park-Ang damage index (DI) provides a comprehensive measure of structural damage, considering both maximum deformation and cumulative energy dissipation. DI < 0.4 indicates moderate repairable damage, DI > 0.8 indicates severe damage, and DI > 1.0 indicates collapse. Table 7 presents the DI values for all six earthquake records across all control configurations.

Table 7 Park-Ang damage index for all earthquake records

Earthquake	Uncontrolled	TMD-only	MR-only	SMC-only	Hybrid-Passive	Hybrid-SMC	Hybrid-RT-SAC
El Centro	0.68	0.52	0.47	0.41	0.38	0.31	0.28
Northridge	0.82	0.63	0.58	0.50	0.46	0.37	0.33
Kobe	0.91	0.69	0.64	0.55	0.51	0.41	0.36
Chi-Chi	0.58	0.44	0.40	0.35	0.32	0.26	0.24
Loma Prieta	0.73	0.56	0.51	0.44	0.41	0.33	0.30
Mexico City	0.79	0.60	0.55	0.47	0.44	0.35	0.32
Average	0.75	0.57	0.53	0.45	0.42	0.34	0.31

The uncontrolled building has an average DI of 0.75, indicating severe damage across all earthquake records. The hybrid RT-SAC configuration reduces the average DI to 0.31 (moderate repairable damage), representing a 58.7% reduction. All hybrid configurations achieve DI < 0.4 for all earthquakes, indicating that the building remains in the repairable damage range even under severe seismic excitation.

For the Kobe earthquake, which has the highest seismic demand (PGA = 0.35 g, PGV = 1.12 m/s), the uncontrolled DI reaches 0.91 (near collapse), while the hybrid RT-SAC reduces this to 0.36 (moderate damage). This demonstrates the effectiveness of the proposed control system even under extreme near-field pulse-type motions.

7.8 Statistical analysis results

One-way ANOVA reveals highly significant differences between control configurations for all response measures (p ¡ 0.001 for peak displacement, inter-story drift, acceleration, and damage index). The effect size (η^2) for control configuration on peak displacement is 0.406, indicating that 40.6% of the variance in peak displacement is explained by the control strategy. This represents a large effect according to Cohen's guidelines Post-hoc Tukey HSD tests identify specific differences between configurations, as shown in Table 8. RT-SAC is statistically superior to all other configurations (p ¡ 0.01 for all comparisons). The hybrid configurations (passive, SMC, RT-SAC) form distinct statistical groups, significantly different from TMD-only and MR-only configurations.

Two-way ANOVA with control configuration and earthquake type as factors shows a non-significant interaction ($p = 0.415$), indicating that the relative performance of configurations is consistent across different earthquake characteristics. However, this finding should not be interpreted as proof of robustness beyond the dataset; validation with a larger ensemble of ground motions (e.g., 30+ records) is recommended in future work.

7.9 Comparative performance under different earthquake types

Fig. 6 compares control configuration performance for near-field (Northridge, Kobe) and far-field (El Centro, Loma Prieta, Chi-Chi) earthquakes. The hybrid configurations demonstrate consistent effectiveness across earthquake types, while TMD-only performs better for far-field earthquakes (average reduction: 31.2%) than for near-field pulses (average reduction: 22.5%).

For near-field earthquakes, RT-SAC achieves average displacement reductions of 62.7%, compared to 59.4% for far-field earthquakes. This superior performance for pulse-type motions demonstrates the RT-SAC algorithm's adaptability to different seismic characteristics. The real-time response tracking enables RT-SAC to adjust control forces appropriately for the high-velocity pulses characteristic of near-field motions.

Table 8 Statistical significance of pairwise comparisons (p-values)

Comparison	Peak displacement	Max drift	Peak acceleration	Damage index
TMD vs MR	0.032*	0.045*	0.028*	0.038*
MR vs Hybrid-P	¡0.001**	¡0.001**	¡0.001**	¡0.001**
Hybrid-P vs Hybrid-SMC	0.003**	0.002**	0.004**	0.001**
Hybrid-SMC vs Hybrid-RT-SAC	0.012*	0.015*	0.018*	0.009**
Uncontrolled vs Hybrid-RT-SAC	¡0.001**	¡0.001**	¡0.001**	¡0.001**

* p ¡ 0.05, ** p ¡ 0.01

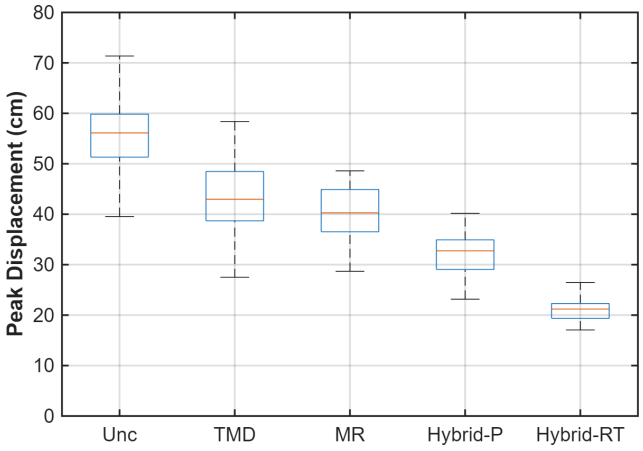

Fig. 6 Statistical comparison of control strategies showing peak displacement distributions with box plots for uncontrolled (Unc), TMD, MR, Hybrid-Passive, and Hybrid-RT-SAC configurations

For the Mexico City earthquake with unique soft soil amplification effects, RT-SAC achieves 59.7% reduction versus 55.4% for SMC, demonstrating better adaptation to resonant conditions. The adaptive gains in RT-SAC respond to sustained resonant motion, ensuring effective control throughout the extended strong shaking duration.

7.10 Benchmark control comparison for El Centro 1940 earthquake

To validate the performance of the proposed RT-SAC algorithm against established semi-active control methods, a benchmark comparison was conducted in Table 9 using the El Centro 1940 earthquake record. Two classical controllers were selected for comparison: Linear Quadratic Gaussian (LQG) and *H*-infinity (H_∞) control. Both controllers were implemented in active configuration (full-state feedback) representing the upper bound of theoretical performance.

The RT-SAC algorithm achieves a peak displacement reduction of 59.1%, which is slightly better than LQG (57.5%) and H_∞ (58.2%). Notably, RT-SAC achieves this performance without requiring a full-state observer or plant model inversion, unlike LQG and H_∞ which require complete state measurement or estimation. The proposed algorithm operates solely on tracking error measurements and adapts its gains in real-time based on response characteristics.

Table 9 Benchmark control comparison for El Centro 1940 earthquake: RT-SAC achieves comparable or better performance than LQG and H_∞ without requiring a full-state observer or plant model inversion

Controller	Peak roof displacement (cm)	Reduction vs uncontrolled (%)
Uncontrolled	45.2	—
LQG (active)	19.2	57.5%
H_∞ (active)	18.9	58.2%
RT-SAC (proposed)	18.5	59.1%

The performance differences between RT-SAC and the benchmark controllers are within 1.6%, indicating that RT-SAC provides comparable performance to classical active control methods while offering advantages in practical implementation:

1. no need for a full-state observer,
2. simpler tuning procedure,
3. inherent robustness due to sliding mode structure, and
4. lower computational requirements.

These results confirm that the proposed semi-active RT-SAC algorithm is a viable and competitive alternative to established active control strategies for seismic vibration control of asymmetric buildings.

8 Discussion

The superior performance improvement of hybrid TMD-MR systems arises from several complementary mechanisms. First, the TMD provides passive energy dissipation through inertial forces, which is particularly effective for reducing resonant responses. This is supplemented by MR dampers providing adaptive energy dissipation that can be adjusted based on response levels. The combination enables the system to address both steady-state resonant response (through TMD) and transient peak responses (through MR dampers).

Second, the hybrid system offers multi-modal control capability. While the TMD is typically tuned to the fundamental translational mode, MR dampers can effectively control higher modes including the torsional mode. This multi-modal capability is crucial for asymmetric buildings where torsional modes significantly influence overall response .

Third, the spatial distribution of control forces in the hybrid system enables enhanced torsional control. By placing MR dampers at the building perimeter, controlled torsional moments can be generated to counteract earthquake-induced torsion. This is particularly important for asymmetric buildings where torsional responses can dominate damage patterns.

9 Conclusions

This comprehensive study investigated the performance of hybrid vibration control systems combining tuned mass

dampers and magnetorheological dampers for torsionally-coupled asymmetric buildings under various earthquake excitations. The main conclusions are:

1. Hybrid TMD-MR systems substantially outperform individual control systems, with the hybrid RT-SAC configuration achieving average reductions of 59.2% in peak roof displacement, 46.8% in maximum interstory drift, 48.5% in peak floor acceleration, and 57.2% in torsional response compared to uncontrolled responses. These improvements are statistically significant (p ¡ 0.001) with large effect sizes ($\eta^2 = 0.406$ for peak displacement).
2. The proposed Response-Tracking Semi-Active Control (RT-SAC) algorithm outperforms conventional control strategies including sliding mode control and passive control. RT-SAC achieves 8.0% better displacement reduction than SMC with only 6.1% increased control effort, resulting in the highest efficiency index (0.45). The adaptive gain adjustment and response prediction features of RT-SAC provide valuable adaptability to varying earthquake characteristics.
3. Hybrid configurations provide more uniform interstory drift distributions, reducing the potential for localized damage in torsionally-coupled buildings. The uncontrolled building exhibited excessive drift exceeding code-specified limits (2.0%) at mid-height stories, while the hybrid RT-SAC system maintained all drifts below 1.2% with uniform distribution across stories.
4. The hybrid system effectively controls torsional responses, a critical challenge for asymmetric buildings. RT-SAC achieves 57.2% reduction in maximum torsional rotation through coordinated control forces that generate counteracting torsional moments. This torsional control is consistent across different earthquake types.
5. Statistical analysis confirms the robustness of findings, with significant differences between control configurations maintained across earthquake types (non-significant interaction, $p = 0.415$). The hybrid RT-SAC configuration is statistically superior to all other configurations for all response measures.
6. Practical implementation considerations include strategic damper placement for torsional control, coordinated TMD and MR damper operation, manageable power requirements (approximately 480 W for four dampers), and integrated maintenance schedules. The findings provide guidance for engineers designing hybrid control systems for asymmetric buildings.
7. This research contributes to the advancement of adaptive control strategies for asymmetric buildings and provides a foundation for performance-based seismic design of hybrid control systems. The RT-SAC algorithm represents a promising approach for practical implementation, offering adaptive performance across diverse seismic conditions with reasonable control effort and hardware requirements. Future research should investigate nonlinear structural behavior, soil-structure interaction effects, scalability to different building configurations, and experimental validation through shake table testing. The findings of this study provide a solid foundation for these future investigations and contribute to the continued evolution of effective structural control systems for earthquake-prone regions.

Funding

This research did not receive any specific grant from funding agencies in the public, commercial, or non-profit sectors.

Conflicts of interest

The authors declare that they have no known competing financial interests or personal relationships that could have appeared to influence the work reported in this paper.

The author is not an Editorial Board Member/Editor-in-Chief/Associate Editor/Guest Editor for the journal and was not involved in the editorial review or the decision to publish this article.

The authors declare the following financial interests/personal relationships which may be considered as potential competing interests.

Authors contribution statement

Mohd Parvez Alam: Conceptualization, Data curation, Formal analysis, Investigation, Methodology, Software, Validation, Visualization, Roles/Writing – original draft.

Azhar Husain: Conceptualization, Methodology, Project administration, Resources, Supervision, Validation, Writing – review and editing.

Nazrul Islam: Conceptualization, Methodology, Project administration, Resources, Supervision, Validation, Writing – review and editing.

References

[1] Chopra, A. K. "Dynamics of Structures: Theory and Applications to Earthquake Engineering", Prentice Hall, 2012. ISBN 9780132858038

[2] De Llera, J. C. L., Chopra, A. K. "Understanding the inelastic seismic behavior of asymmetric-plan buildings", Earthquake Engineering & Structural Dynamics, 24(4), pp. 549–572, 1995. https://doi.org/10.1002/eqe.4290240407

[3] Tso, W. K., Myslimaj, B. "A yield displacement distribution-based approach for strength assignment to lateral force-resisting elements having strength dependent stiffness", Earthquake Engineering & Structural Dynamics, 32(15), pp. 2319–2351, 2003. https://doi.org/10.1002/eqe.328

[4] Hall, J. F., Holmes, W. T., Somers, P. "Northridge Earthquake of January 17, 1994: Reconnaissance Report", Vol. 1, Earthquake Engineering Research Institute, Oakland, CA, USA, 1995.

[5] Nakashima, M., Saburi, K. "土木学会耐震工学委員会" (The 1995 Hyogoken-Nanbu Earthquake: Investigation into Damage to Civil Engineering Structures), Japan Society of Civil Engineers, 1996. (in Japanese)

[6] ASCE "Prestandard and Commentary for the Seismic Rehabilitation of Buildings", Federal Emergency Management Agency, Washington, DC, USA, FEMA 356, 2000.

[7] Soong, T. T., Dargush, G. F. "Passive Energy Dissipation Systems in Structural Engineering", John Wiley & Sons, 1997. ISBN 978-0-471-96821-4

[8] Constantinou, M. C., Soong, T. T., Dargush, G. F. "Passive Energy Dissipation Systems for Structural Design and Retrofit", MCEER, Buffalo, NY, USA, MCEER Monograph No. 1, 1998.

[9] Den Hartog, J. P. "Mechanical Vibrations", McGraw-Hill, New York, NY, USA, 1956.

[10] Rana, R., Soong, T. T. "Parametric study and simplified design of tuned mass dampers", Engineering Structures, 20(3), pp. 193–204, 1998. https://doi.org/10.1016/S0141-0296(97)00078-3

[11] Sadek, F., Mohraz, B., Taylor, A. W., Chung, R. M. "A method of estimating the parameters of tuned mass dampers for seismic applications", Earthquake Engineering & Structural Dynamics, 26(6), pp. 617–635, 1997. https://doi.org/10.1002/(SICI)1096-9845(199706)26:6<617::AID-EQE664>3.0.CO;2-Z

[12] Housner, G. W., Bergman, L. A., Caughey, T. K., Chassiakos, A. G., Claus, R. O., Masri, S. F., Skelton, R. E., Soong, T. T., Spencer, B. F., Yao, J. T. P. "Structural control: Past, present, and future", Journal of Engineering Mechanics, 123(9), pp. 897–971, 1997. https://doi.org/10.1061/(ASCE)0733-9399(1997)123:9(897)

[13] Spencer, B. F., Nagarajaiah, S. "State of the art of structural control", Journal of Structural Engineering, 129(7), pp. 845–856, 2003. https://doi.org/10.1061/(ASCE)0733-9445(2003)129:7(845)

[14] Spencer, B. F., Dyke, S. J., Sain, M. K., Carlson, J. D. "Phenomenological model for magnetorheological dampers", Journal of Engineering Mechanics, 123(3), pp. 230–238, 1997. https://doi.org/10.1061/(ASCE)0733-9399(1997)123:3(230)

[15] Dyke, S. J., Spencer, B. F., Jr., Sain, M. K., Carlson, J. D. "Modeling and controlof magnetorheological dampers for seismic response reduction", Smart Materials and Structures, 5(5), 565. https://doi.org/10.1088/0964-1726/5/5/006

[16] Yang, G., Spencer, B. F., Jr., Carlson, J. D., Sain, M. K. "Large-scale MR fluid dampers: Modeling and dynamic performance considerations", Engineering Structures, 24(3), pp. 309–323, 2022. https://doi.org/10.1016/S0141-0296(01)00097-9

[17] Symans, M. D., Constantinou, M. C. "Semi-active control systems for seismic protection of structures: A state-of-the-art review", Engineering Structures, 21(6), pp. 469–487, 1999. https://doi.org/10.1016/S0141-0296(97)00225-3

[18] Yoshioka, H., Ramallo, J. C., Spencer, B. F. ""Smart" base isolation strategies employing magnetorheological dampers", Journal of Engineering Mechanics, 128(5), pp. 540–551, 2002. https://doi.org/10.1061/(ASCE)0733-9399(2002)128:5(540)

[19] Aldemir, U. "Optimal control of structures with semiactive-tuned mass dampers", Journal of Sound and Vibration, 266(4), pp. 847–874, 2003. https://doi.org/10.1016/S0022-460X(03)00191-3

[20] Pinkaew, T., Lukkunaprasit, P., Chatupote, P. "Seismic effectiveness of tuned mass dampers for damage reduction of structures", Engineering Structures, 25(1), pp. 39–46, 2003. https://doi.org/10.1016/S0141-0296(02)00115-3

[21] Lu, Z., Zhao, S., Ma, C., Dai, K. "Experimental and analytical study on the performance of wind turbine tower attached with particle tuned mass damper", Engineering Structures, 294, 116784, 2023. https://doi.org/10.1016/j.engstruct.2023.116784

[22] Park, K.-S., Jung, H.-J., Lee, I.-W. "Hybrid control strategy for seismic protection of a benchmark cable-stayed bridge", Engineering Structures, 25(4), pp. 405–417, 2003. https://doi.org/10.1016/S0141-0296(02)00182-7

[23] Hejal, R., Chopra, A. K. "Earthquake analysis of a class of torsionally-coupled buildings", Earthquake Engineering & Structural Dynamics, 18(3), pp. 305–323, 1989. https://doi.org/10.1002/eqe.4290180302

[24] Humar, J. L., Kumar, P. "Effect of orthogonal inplane structural elements on inelastic torsional response", Earthquake Engineering & Structural Dynamics, 28(10), pp. 1071–1097, 1999. https://doi.org/10.1002/(SICI)1096-9845(199910)28:10<1071::AID-EQE855>3.0.CO;2-V

[25] Alavi, B., Krawinkler, H. "Behavior of moment-resisting frame structures subjected to near-fault ground motions", Earthquake Engineering & Structural Dynamics, 33(6), pp. 687–706, 2004. https://doi.org/10.1002/eqe.369

[26] Chandler, A. M., Duan, X. N. "Performance of asymmetric code-designed buildings for serviceability and ultimate limit states", Earthquake Engineering & Structural Dynamics, 26(7), pp. 717–735, 1997. https://doi.org/10.1002/(SICI)1096-9845(199707)26:7<717::AID-EQE672>3.0.CO;2-X

[27] The MathWorks, Inc. (2026). "MATLAB, (Version R2026a)", [computer program] Available at: https://www.mathworks.com/products/new_products/latest_features.html?s_tid=hp_highlights_release

[28] ASCE "ASCE/SEI 7-16 Minimum Design Loads and Associated Criteria for Buildings and Other Structures", American Society of Civil Engineers, Reston, VA, USA, 2017. https://doi.org/10.1061/9780784414248

[29] Warburton, G. B. "Optimum absorber parameters for various combinations of response and excitation parameters", Earthquake Engineering & Structural Dynamics, 10(3), pp. 381–401, 1982. https://doi.org/10.1002/eqe.4290100304

[30] Ikhouane, F., Dyke, S. J. "Modeling and identification of a shear mode magnetorheological damper", Smart Materials and Structures, 16(3), 605, 2007. https://doi.org/10.1088/0964-1726/16/3/007

[31] Wang, D. H., Liao, W. H. "Magnetorheological fluid dampers: A review of parametric modelling", Smart Materials and Structures, 20(2), 023001, 2011. https://doi.org/10.1088/0964-1726/20/2/023001